LAWRENCE
LIVERMORE
NATIONAL
LABORATORY

LLNL-JRNL-845315

Tropospheric Temperature [in "State of the Climate in 2022"]

S. Po-Chedley, J. R. Christy, C. Z. Zou, C. A. Mears, L. Haimberger

February 17, 2023

Bulletin of the American Meteorological Society

Disclaimer

Tropospheric temperature [in State of the Climate in 2022]

Po-Chedley, Stephen, Lawrence Livermore National Laboratory, Livermore, California
Christy, John R., University of Alabama in Huntsville, Huntsville, Alabama
Zou, Cheng-Zhi, NOAA/NESDIS Center for Satellite Applications and Research, College Park, Maryland
Mears, Carl A., Remote Sensing Systems, Santa Rosa, California
Haimberger, Leopold, University of Vienna, Vienna, Austria

The 2022 globally averaged lower-tropospheric temperature (LTT) anomaly was +0.26°C (+0.17 to +0.37°C) higher than the 1991–2020 average, ranking among the nine warmest years on record (fourth to ninth warmest, depending on the dataset). Long-term warming of the troposphere is consistent with our understanding of greenhouse warming. Other factors, such as volcanic eruptions, decadal variability, and solar activity also modulate the long-term warming trend (Christy and McNider 2017; Po-Chedley et al. 2022). Interannual variations in global LTT are dominated by the El Niño-Southern Oscillation, which has largely been in a La Niña state since August 2020 (see section 4b; Figs. 2.b.5.1a,b). As with the year 2021, the depression of atmospheric temperature due to La Niña combined with the background warming trend (Table 2.b.5.1) produced a year that was warmer-than-average, but not record-breaking.

La Niña events are accompanied by a distinct pattern of tropospheric temperature anomalies, which are evident in the annual average departures in both 2022 (Plate 2.1) and 2021 (see Plate

2.1f in Blunden and Boyer 2022). La Niña conditions over late 2021 through 2022 contributed to record-breaking LTT values over the North and South Pacific Ocean, China, and parts of South Asia. Persistent summertime heatwaves during June to August contributed to record-breaking tropospheric temperatures over Europe in 2022. Large positive total column water vapor anomalies were collocated with the anomalous tropospheric warmth (Plate 2.1.z; section 2.d.2). Overall, the global LTT was above average across 70% of the globe, with 6% of Earth experiencing the highest temperatures since the start of the record in 1979 (Plate 2.1; Fig. 2.b.5.1c). In contrast, 1% of Earth experienced its coldest year on record.

Atmospheric temperature data are derived from balloon-borne radiosonde measurements, satellite-based microwave soundings, and atmospheric reanalyses (Table 2.b.5.1). Each dataset employs different strategies to remove biases and drifts from sources of atmospheric temperature data. Across datasets and measurement techniques, there is good agreement on interannual timescales (Fig. 2.b.5.1a; Supp. Fig. A2.b.5), but structural uncertainty leads to non-negligible difference in long-term warming trends (Table 2.b.5.1).

One issue in the construction of tropospheric temperature microwave records is that short-term trends from overlapping satellites do not always agree after estimated biases are removed. For example, tropospheric warming inferred from the Microwave Sounding Unit (MSU) onboard the NOAA-14 satellite exceeds that from Advanced MSU (AMSU) data from NOAA-15. Reliance on data from NOAA-14 (NOAA-15) results in larger (smaller) estimates of tropospheric warming (Mears and Wentz 2016; Santer et al. 2021). A new version of the NOAA STAR dataset treats data from the latest microwave sounding instruments (AMSU and the Advanced

47 Technology Microwave Sounder) as a reference with which to calibrate earlier data from earlier
48 MSU instruments (Zou et al. 2021, 2023). This decision has the effect of substantially reducing
49 global TTT warming over 1979 to 2021 (from 0.23°C decade^{-1} to 0.14°C decade^{-1}; Zou et al.
50 2023). Changes in the estimated rate of warming of a few hundredths of a degree per decade are
51 common when tropospheric temperature datasets are updated. These changes illustrate the
52 challenges and pronounced structural uncertainty in constructing records of tropospheric
53 warming.
54
55 General circulation models (GCMs) tend to simulate greater tropospheric warming than satellite
56 observations over 1979 to present, particularly in the tropics (McKitrick and Christy 2020; Po-
57 Chedley et al. 2021; Zou et al. 2023). Observed tropical sea surface warming, which is closely
58 coupled to tropospheric warming, is also smaller than the average warming in GCMs (Eyring et
59 al. 2021). Two factors likely contribute to faster-than-observed model warming: biases in the
60 prescribed model forcing and biases in the GCM response to greenhouse gas forcing. For
61 example, Fasullo et al. (2022) shows that a discontinuity in the biomass-burning aerosol forcing
62 prescribed to models in Phase 6 of the Coupled Model Intercomparison Project (CMIP6) results
63 in inflated warming in version 2 of the Community Earth System Model—an issue that may
64 affect other CMIP6 GCMs. Several GCMs also exceed the likely range of estimates of climate
65 sensitivity (Forster et al. 2021)—the global surface warming response to a doubling of
66 atmospheric carbon dioxide—which in turn contributes to overestimates of historical warming
67 (Scafetta 2023). Multidecadal internal variability has also reduced observed warming since 1979
68 (Po-Chedley et al. 2022), which contributes to the difference between observed and simulated

warming. Aside from these factors, it is also possible that observational biases may affect observed tropospheric warming (Santer et al. 2021).

References

Blunden, J. and T. Boyer, Eds., 2022: "State of the Climate in 2021". Bull. Amer. Meteor. Soc., 103 (8), Si–S465, https://doi.org/10.1175/2022BAMSStateoftheClimate.1

Christy, J. R. and R. T. McNider (2017): Satellite Bulk Tropospheric Temperatures as a Metric for Climate Sensitivity, Asia-Pac. J. Atmos. Sci., 53(4) 511-518, doi: 10.1007/s13143-017-0070-z.

Eyring, V., N.P. Gillett, K.M. Achuta Rao, R. Barimalala, M. Barreiro Parrillo, N. Bellouin, C. Cassou, P.J. Durack, Y. Kosaka, S. McGregor, S. Min, O. Morgenstern, and Y. Sun, 2021: Human Influence on the Climate System. In Climate Change 2021: The Physical Science Basis. Contribution of Working Group I to the Sixth Assessment Report of the Intergovernmental Panel on Climate Change [Masson-Delmotte, V., P. Zhai, A. Pirani, S.L. Connors, C. Péan, S. Berger, N. Caud, Y. Chen, L. Goldfarb, M.I. Gomis, M. Huang, K. Leitzell, E. Lonnoy, J.B.R. Matthews, T.K. Maycock, T. Waterfield, O. Yelekçi, R. Yu, and B. Zhou (eds.)]. Cambridge University Press, Cambridge, United Kingdom and New York, NY, USA, pp. 423–552, doi:10.1017/9781009157896.005

Fasullo, J. T., Lamarque, J.-F., Hannay, C., Rosenbloom, N., Tilmes, S., DeRepentigny, P., et al. (2022). Spurious late historical-era warming in CESM2 driven by prescribed biomass burning emissions. *Geophysical Research Letters*, 49, e2021GL097420. https://doi.org/10.1029/2021GL097420.

Forster, P., T. Storelvmo, K. Armour, W. Collins, J.-L. Dufresne, D. Frame, D.J. Lunt, T. Mauritsen, M.D. Palmer, M. Watanabe, M. Wild, and H. Zhang, 2021: The Earth's Energy Budget, Climate Feedbacks, and Climate Sensitivity. In Climate Change 2021: The Physical Science Basis. Contribution of Working Group I to the Sixth Assessment Report of the Intergovernmental Panel on Climate Change [Masson-Delmotte, V., P. Zhai, A. Pirani, S.L. Connors, C. Péan, S. Berger, N. Caud, Y. Chen, L. Goldfarb, M.I. Gomis, M. Huang, K. Leitzell, E. Lonnoy, J.B.R. Matthews, T.K. Maycock, T. Waterfield, O. Yelekçi, R. Yu, and B. Zhou (eds.)]. Cambridge University Press, Cambridge, United Kingdom and New York, NY, USA, pp. 923–1054, doi:10.1017/9781009157896.009.

Free, M., D.J. Seidel, J.K. Angel, J. Lanzante, I. Durre and T.C. Peterson, (2005): Radiosonde Atmospheric Temperature Products for Assessing Climate (RATPAC): A new dataset of large-area anomaly time series. *Journal of Geophysical Research*, **110**, D22101, 10.1029/2005JD006169.

Gelaro, R., W. McCarty, M.J. Suárez, R. Todling, A. Molod, L. Takacs, C.A. Randles, A. Darmenov, M.G. Bosilovich, R. Reichle, K. Wargan, L. Coy, R. Cullather, C. Draper, S. Akella, V. Buchard, A. Conaty, A.M. da Silva, W. Gu, G. Kim, R. Koster, R. Lucchesi, D. Merkova, J.E. Nielsen, G. Partyka, S. Pawson, W. Putman, M. Rienecker, S.D. Schubert,

M. Sienkiewicz, and B. Zhao, 2017: The Modern-Era Retrospective Analysis for Research and Applications, Version 2 (MERRA-2). J. Climate, 30, 5419–5454, https://doi.org/10.1175/JCLI-D-16-0758.1

Haimberger, L., C. Tavolato, and S. Sperka (2012). Homogenization of the Global Radiosonde Temperature dataset through combined comparison with reanalysis background series and neighboring stations. *J. Climate*, **25**, 8108– 8131, doi: 10.1175/JCLI-D-11-00668.1.

Hersbach, H, Bell, B, Berrisford, P, et al. (2020). The ERA5 global reanalysis. *Q. J. R. Meteorol. Soc.*, **146,** 1999– 2049, doi: 10.1002/qj.3803.

Kobayashi, S., Y. Ota, Y. Harada, A. Ebita, M. Moriya, H. Onoda, K. Onogi, H. Kamahori, C. Kobayashi, H. Endo, K. Miyaoka, K. Takahashi, 2015: The JRA-55 Reanalysis: General Specifications and Basic Characteristics. J. Meteorol. Soc. Japan, 93, 5-48, doi:10.2151/jmsj.2015-001.

McKitrick, R., & Christy, J. (2020). Pervasive Warming Bias in CMIP6 Tropospheric Layers. *Earth and Space Science*, **7**(9). doi: 0.1029/2020ea001281.

Mears, C. A. and F. J. Wentz, 2016: Sensitivity of satellite-derived tropospheric temperature trends to the diurnal cycle adjustment. *J. Climate*, **29**, 3629–3646, doi: 10.1175/JCLI-D-15-0744.1.

Po-Chedley, S., Thorsen, T. J., & Fu, Q. (2015). Removing Diurnal Cycle Contamination in Satellite-Derived Tropospheric Temperatures: Understanding Tropical Tropospheric Trend Discrepancies. *Journal of Climate*, **28**(6), 2274–2290, doi: 10.1175/jcli-d-13-00767.1

Po-Chedley, S., B. D. Santer, S. Fueglistaler, M. D. Zelinka, P. J. Cameron-Smith, J. Painter, and Q. Fu (2021). Natural variability contributes to model-satellite differences in tropical tropospheric warming. *Proceedings of the Natural Academy of Sciences*, **118**, e2020962118, doi: 10.1073/pnas.2020962118.

Po-Chedley, S., J. T. Fasullo, N. Siler, E. A. Barnes, Z. M. Labe, C. J. W. Bonfils, B. D. Santer, 2022: Internal variability and forcing influence model-satellite differences in the rate of tropical tropospheric warming. *Proceedings of the National Academy of Sciences,* **119** (47) e2209431119, doi: 10.1073/pnas.2209431119.

Rayner N. A., D. E. Parker, E. B. Horton, C. K. Folland, L. V. Alexander, D. P. Rowell, E. C. Kent, A. Kaplan (2003): Global analyses of sea surface temperature, sea ice, and night marine air temperature since the late nineteenth century, *J. Geophys. Res.*, **108** (D14), 4407, doi:10.1029/2002JD002670.

Santer, B. D., S. Po-Chedley, C. Mears, J. C. Fyfe, N. Gillett, Q. Fu, J. F. Painter, S. Solomon, A. K. Steiner, F. J. Wentz, M. D. Zelinka, and C.-Z. Zou (2021). Using Climate Model Simulations to Constrain Observations. *Journal of Climate*, **34**, 6281 –6301, doi: 10.1175/JCLI-D-20-0768.1.

Scafetta, N. (2023): CMIP6 GCM ensemble members versus global surface temperatures. *Clim Dyn* **60**, 3091–3120, doi: 10.1007/s00382-022-06493-w

Spencer, R. W., Christy, J. R., & Braswell, W. D. (2017). UAH Version 6 global satellite temperature products: Methodology and results. *Asia-Pacific Journal of Atmospheric Sciences*, **53**(1), 121–130, doi: 10.1007/s13143-017-0010-y.

Zou, C.-Z., H. Xu, X. Hao, and Q. Fu (2021). Post-Millennium Atmospheric Temperature Trends Observed From Satellites in Stable Orbits. *Geophys. Res. Lett.*, **48**, e2021GL093291.

Zou, C.-Z., H. Xu, X. Hao, Q. Liu (2023). Mid-Tropospheric Layer Temperature Record Derived from Satellite Microwave Observations with Backward Merging Approach. *J. Geophys. Res.*, **128**, e2022JD037472, doi: 10.1029/2022JD037472.

Tables

Table 2.b.5.1. Temperature trends (units of °C decade^{-1}) for global lower tropospheric temperature (LTT) and tropical tropospheric temperature (TTT) over the periods 1958–2022 and 1979–2022. NASA MERRA-2 data begins in 1980 and NOAA STAR v5.0 TLT begins in 1981. UW and NOAA STAR do not produce LTT products.

		LTT (90°S–90°N)		TTT (20°S–20°N)	
Start Year		1958	1979	1958	1979
Radiosonde	NOAA RATPAC vA2 (Free et al. 2005)	0.18	0.22	0.17	0.18
	RAOBCORE v1.9 (Haimberger et al. 2012)	0.16	0.17	0.13	0.15
	RICH v1.9 (Haimberger et al. 2012)	0.18	0.20	0.18	0.19
Satellite	UAH v6.0 (Spencer et al. 2017)	–	0.13[1]	–	0.12
	RSS v4.0 (Mears and Wentz, 2016)	–	0.21	–	0.16
	UW v1.0 (Po-Chedley et al. 2015)	–	–	–	0.16
	NOAA STAR v5.0 (Zou et al. 2023)	–	0.13[1]	–	0.10
Reanalysis	ERA5 (Hersbach et al. 2020)	–	0.18	–	0.15
	JRA-55 (Kobayashi et al. 2015)	0.17	0.18	0.16	0.14
	NASA MERRA-2 (Gelaro et al. 2017)	–	0.19	–	0.17
Median		0.17	0.18	0.16	0.15

[1] The vertical sampling in UAH and STAR LTT is slightly different from other datasets and results in temperature trends that are approximately 0.01°C decade^{-1} smaller than other datasets.

Figures

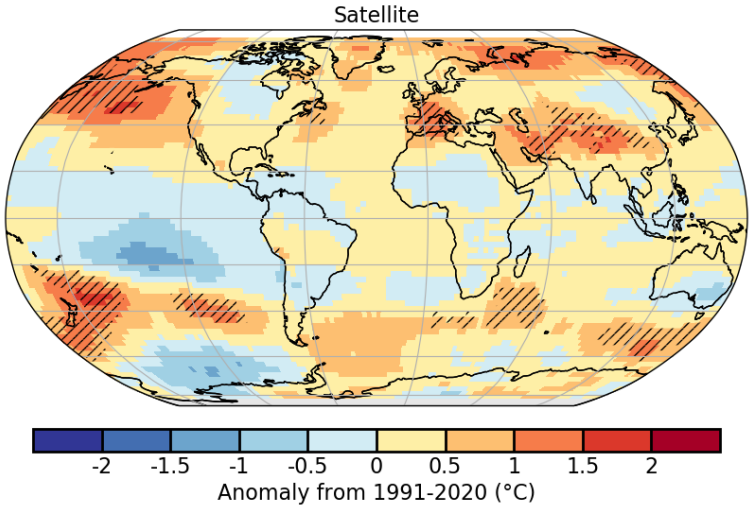

Plate 2.1. Annual average of RSS and UAH lower-tropospheric temperature anomalies for 2022. Hatching denotes regions in which 2022 was the warmest year on record.

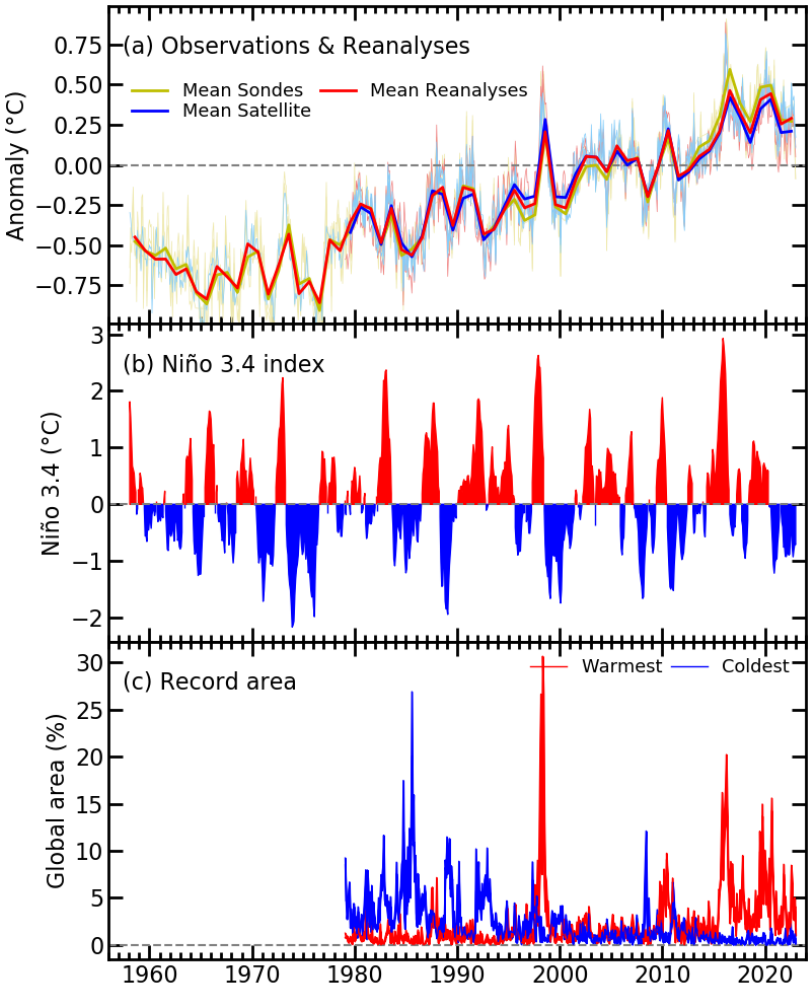

Fig. 2.b.5.1. Time series of (a) global average lower tropospheric temperature (LTT; °C) anomalies, (b) central Pacific (Niño 3.4 region) sea surface temperature anomalies (°C), and (c) percentage of Earth experiencing record high (red) and low (blue) LTT values, according to RSS and UAH LTT datasets for the period 1979–2022. Bold lines in (a) represent the annual average values (across datasets) for reanalysis (teal) and satellite (blue) data. Monthly values for individual datasets are also plotted with thinner and lighter lines for context. The climatological base period for (a) and (b) is 1991–2020. Niño 3.4 anomalies are calculated using the HadISST1 dataset (Rayner et al. [2003]). STAR data is not included in the satellite LTT time series because the time series begins in 1981 (versus 1979 for RSS and UAH data).

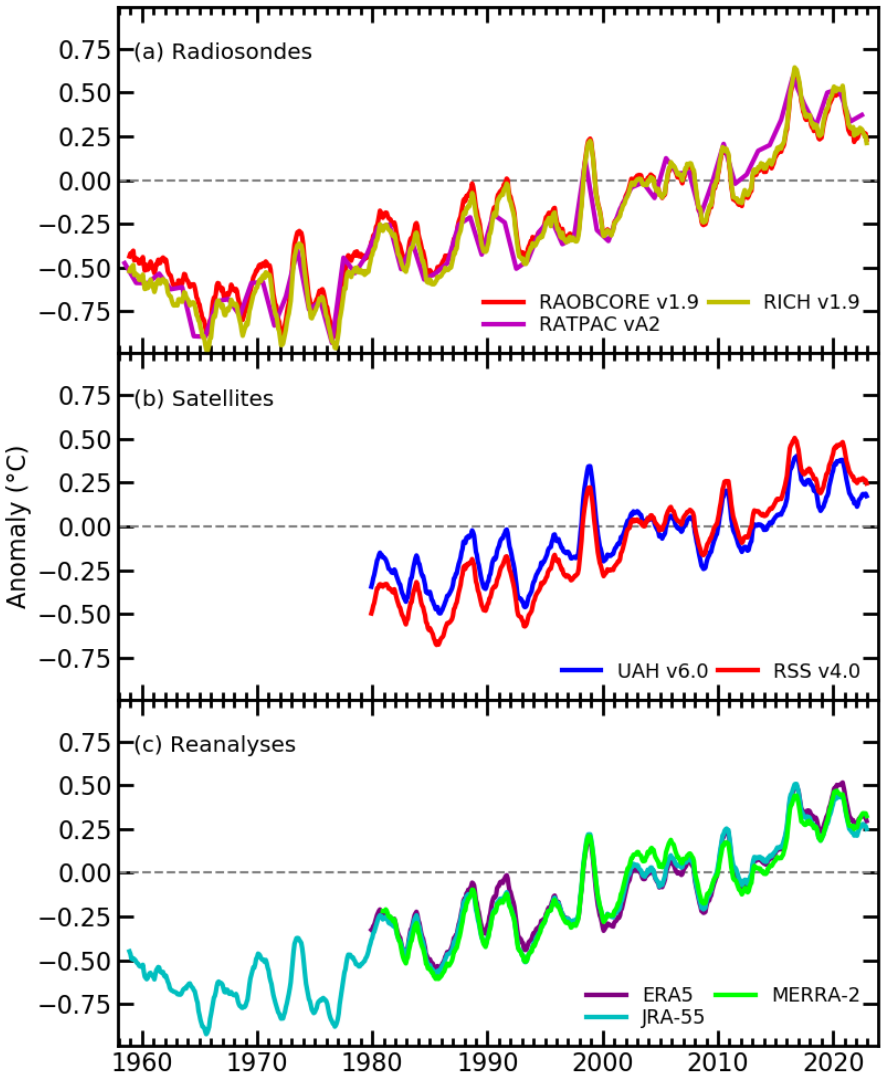

Fig. A2.b.5.1. Monthly average global lower tropospheric temperature (LTT) anomalies for (a) radiosonde, (b) satellite, and (c) reanalysis datasets. Time series are smoothed using a 12-month running average. Annual averages are displayed for the RATPAC dataset. Anomalies are with respect to a 1991–2020 base period.

Datasets

RATPAC vA2: https://www1.ncdc.noaa.gov/pub/data/ratpac/

RICH v1.9: https://srvx1.img.univie.ac.at/webdata/haimberger/v1.9/

RAOBCORE v1.9: https://srvx1.img.univie.ac.at/webdata/haimberger/v1.9/

UAH v6.0: https://www.nsstc.uah.edu/data/msu/v6.0/

UW v1.0: https://pochedls.github.io/

RSS v4.0: http://www.remss.com/measurements/upper-air-temperature/

NOAA STAR v5.0:

https://www.star.nesdis.noaa.gov/pub/smcd/emb/mscat/data/MSU_AMSU_v5.0/Monthly_Atmospheric_Layer_Mean_Temperature/

MERRA-2: https://gmao.gsfc.nasa.gov/reanalysis/MERRA-2/data_access/

JRA-55: https://rda.ucar.edu/datasets/ds628.1/

ERA5: https://cds.climate.copernicus.eu/cdsapp#!/dataset/reanalysis-era5-pressure-levels-monthly-means

Niño 3.4 data: https://psl.noaa.gov/gcos_wgsp/Timeseries/Nino34/

Acknowledgements

Work performed by Stephen Po-Chedley at Lawrence Livermore National Laboratory (LLNL) was supported by LDRD 23-FS-009 and performed under the auspices of the DOE under Contract DE-AC52-07NA27344. IM release: LLNL-JRNL-845315.